How fluctuation intensity flux drives SOL expansion

To cite this article before publication: Nami Li *et al* 2023 *Nucl. Fusion* in press https://doi.org/10.1088/1741-4326/ad0599

How Fluctuation Intensity Flux Drives SOL Expansion

Nami Li[1*], X.Q. Xu[1], P.H. Diamond[2], T. Zhang[3], X. Liu[3], Y. F. Wang[3], N. Yan[3] and G.S. Xu[3]

[1]*Lawrence Livermore National Laboratory, Livermore, CA 94550, USA*
[2]*University of California San Diego, La Jolla, CA 92093-0429, USA*
[3]*Institute of Plasma Physics, Chinese Academy of Sciences, Hefei 230031, China*
li55@llnl.gov

Abstract

Predictions of heat load widths λ_q based on particle orbits alone are very pessimistic. This paper shows that pedestal peeling-ballooning (P-B) MHD turbulence broadens the stable SOL by the transport, or spreading, of fluctuation energy from the pedestal. λ_q is seen to increase with Γ_ε, the fluctuation energy density flux. We elucidate the fundamental physics of the spreading process. Γ_ε increases with pressure fluctuation correlation length. P-B turbulence is seen to be especially effective at spreading, on account of its large effective mixing length. Spreading is shown to be a multiscale process, which is enhanced by the synergy of large and small-scale modes. Pressure fluctuation skewness correlates well with the spreading flux – with the zero crossing of skewness and Γ_ε spatially coincident – suggesting the role of coherent fluctuation structures and the presence of intermittency in λ_q broadening. $\lambda_q \sim B_p^{-1}$ scaling persists for the broadened SOL. We show that the spreading flux increases for increasing pedestal pressure gradient ∇P_0 and for decreasing pedestal collisionality υ_{ped}^*. This trend is due to the dominance of peeling modes for large ∇P_0 and low υ_{ped}^*. Ultimately, we see that a state of weak MHD turbulence, as for small ELMs, is very attractive for heat load management. Our findings have transformative implications for future fusion reactor designs and call for experimental investigations to validate the observed trends.

Entrainment, the tendency of a patch of turbulence to expand into a neighboring laminar region, is a well-known phenomenon. A classic example of entrainment is the turbulent wake,[1] which expands or 'spreads' behind a moving object such as a boat, and expands downstream (distance ~x) with width $w \sim x^{1/3}$. Entrainment is a mixing process, where a turbulent region invades and mixes into a laminar region. Thus, entrainment is naturally characterized by a mixing length which is considered as the distance traversed by a fluid mass before it loses its individuality by mixing with neighboring masses,[2] related to the characteristic length scale of the turbulence. Entrainment occurs in wakes, boundary layers and jets, and in similar phenomena in plasma physics, where it is called turbulence spreading.[3-11] Since the interface between laminar and turbulent regions are likely to be multi-fractal, mean field theory approaches are limited, and descriptions of entrainment involving jets,[12] avalanching[13] and directed percolation[14] have been developed.

In this paper, we show how the magnetohydrodynamics (MHD) turbulent core (specifically the pedestal) of a plasma confinement device can entrain an otherwise laminar boundary (i.e. scrape-off layer (SOL)), thus naturally broadening or thickening the latter. This is of great interest, since such a broadened boundary (SOL) enables a broader distribution of the heat load on the plasma facing components, specifically on tokamak divertor plates. Significantly, this work represents the first simulation/modelling endeavor to incorporate the convective transport of fluctuation energy, which distinguish it from the predominantly diffusive mechanism employed in previous published models.

Improved confinement in H-mode leads to ExB shear suppression of SOL turbulence. As a consequence, heat load width collapses to unacceptably narrow sizes. This trend is captured by pessimistic scalings predicted by the heuristic drift-based model (HD model)[15] and ITPA multi-machine experimental (Eich) scaling law[16], in which the SOL width λ_q is inversely proportional to the poloidal magnetic field B_p in low-gas-puff H-mode tokamak plasmas. Extrapolation to ITER leads to pessimistic results, with $\lambda_q \leq 1mm$.

Recently, both experiments and simulations show that in small/grassy ELMs regimes, the ELM size remains small but the SOL width λ_q is broadened, while high plasma confinement persists, in contrast to the case of type-I ELMs[17-23]. Here ELMs stand for the edge-localized modes, being characterized by quasi-periodic relaxation events occurring at the edge pedestal H-mode plasmas. Experimental observations from AUG and JET show the broadening of λ_q for H-mode plasma with high separatrix density or collisionality[24-26]. The mechanisms for the λ_q broadening in the high density/collisionality regimes are: 1) parallel confinement time in the SOL is enhanced due to large thermal resistivity at high collisionality[27, 28]; 2) perpendicular transport is enhanced by the onset of additional instabilities in the SOL, such as resistive magnetohydrodynamic (MHD) modes, etc.[29] In addition, simulations by the XGC1 and BOUT++ codes predict a significant broadening of λ_q for ITER[30, 31], on account of enhanced radial transport. BOUT++ transport simulations confirm that a transition from magnetic drift to turbulent transport regime occurs as the turbulent cross-field diffusivity increases.[31-33] Even though both XGC and BOUT++ simulations claimed victory for ITER, they did not identify or elucidate the physical mechanism underpinning SOL broadening. *In this paper, we show that in the small/grassy ELM regime, the SOL width is significantly broadened by turbulence spreading from the pedestal to the SOL.* Along the way, we see that the peak divertor heat flux is much smaller than that for type-I ELMs, and fundamental physics of the spreading process is elucidated.

EAST experiments show that there is a strong relationship between the divertor particle flux width λ_{js} and upstream density fluctuation level S_{fluc} near the separatrix, as shown by Fig. 1. Here the data are the results of statistical average calculation based on multiple discharges with the similar parameters as listed in this letter. In the ELM free regime, the density fluctuation level is

low, and λ_{js} remains steady (blue squares). This is comparable with that for inter-Large ELM regime (black crosses) and is also consistent with the prediction made by the HD model. Upon entering the grassy ELM regime, the density fluctuation increases, and the divertor particle flux width increases concurrently. This suggests that turbulence may be at work broadening the SOL. However, this requires the transport of turbulence energy into the SOL. The question remains though, what is the physics mechanism underpinning the SOL width broadening driven by turbulence? *Thus, we turn our attention to turbulence spreading.* In this letter, we use BOUT++[34] turbulence nonlinear simulations to investigate the impact of turbulent transport on heat flux width broadening, for the specific four EAST experimental discharges with shots #103751, #103745, #103748 and #090949.[19, 35] *We show that turbulence spreading is responsible for heat load broadening*, and that SOL broadening is enhanced for steep pedestal pressure gradient and low collisionality.

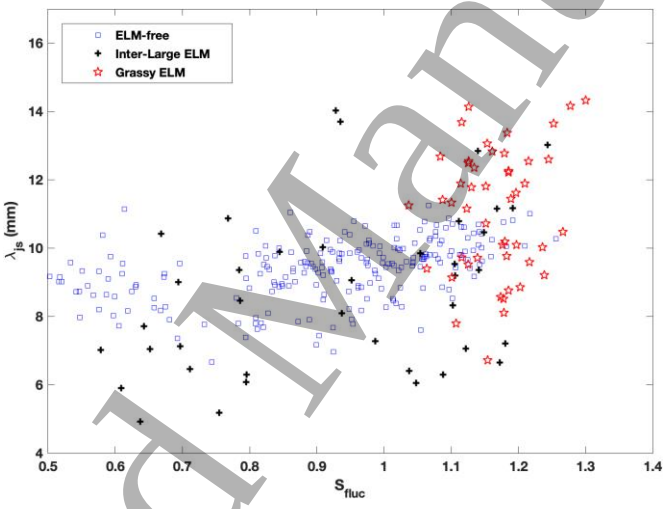

Fig. 1. The divertor particle flux width vs density fluctuation at outer midplane near the separatrix for EAST ELM-free (blue squares), inter-Large ELM (black crosses) and grassy ELM (red stars).

Physics model – To study turbulence spreading from the pedestal to the SOL, a simple model is used to identify the key physical variables for the SOL width broadening. Let us consider only the radial convective evolution of the pressure equation:

$$\frac{\partial p}{\partial t} = -\nabla \cdot (\boldsymbol{v} p) \tag{1}$$

$$p = \langle p \rangle + \tilde{p} \tag{2}$$

Here the damping and cross-field coupling are neglected. Fluctuations are defined by taking the difference to the zonal and time average $\langle \cdot \rangle = \int d\theta d\psi dt$ as the mean quantity $\tilde{p} = p - \langle p \rangle$. For simplicity, the radial background flow is neglected ($\langle v_r \rangle = 0$) and the plasma turbulence flow is treated as incompressible, with $\frac{\partial}{\partial r}\widetilde{v_r} + \frac{1}{r}\frac{\partial}{\partial \theta}\widetilde{v_\theta} = 0$. The evolution of the mean pressure, neglecting sources, sinks and dissipation for simplicity, is given by:

$$\frac{\partial\langle p\rangle}{\partial t} = -\frac{\partial}{\partial r}\langle\tilde{v_r}p\rangle = -\frac{\partial}{\partial r}\langle\tilde{v_r}\tilde{p}\,\rangle \tag{3}$$

The evolution of the turbulence energy can be thus derived as follows:

$$\frac{1}{2}\frac{\partial\langle\tilde{p}^2\rangle}{\partial t} = -\langle\tilde{v_r}\tilde{p}\rangle\frac{\partial}{\partial r}\langle p\rangle - \frac{1}{2}\frac{\partial}{\partial r}\langle\tilde{v_r}\tilde{p}^2\rangle \tag{4}$$

The first term on the right-hand side in Eq. (4) represents energy transfer from the mean field to the turbulence. This term accounts for the local drive of turbulence in the SOL. The second term corresponds to the divergence of a flux $\Gamma_e = \langle\tilde{v_r}\tilde{p}^2\rangle$, which signifies the transport of the fluctuation intensity from the pedestal to the SOL, effectively transfer it from unstable to stable regions. This term characterizes the spreading of turbulence, while the flux itself Γ_p, is specifically recognized as the fluctuation energy density flux $\Gamma_\varepsilon = c_s^2\langle\tilde{v_r}(\tilde{p}/p_0)^2\rangle = (c_s^2/p_0^2)\Gamma_e$. Here c_s is the sound speed, $p_0$is the equilibrium pressure. To compare these two processes, we introduce the production ratio $R_a = \Gamma_e/P_{sol}$, which is the ratio of spreading $\Gamma_e = \int_{sep}^{SOL} -\frac{\partial}{\partial \mathrm{r}}\langle\tilde{\mathrm{v}}_\mathrm{r}\tilde{\mathrm{p}}^2\rangle dr = \langle\tilde{v_r}\tilde{p}^2\rangle|_{sep}$ from pedestal to the SOL to the locally initiated turbulence production $P_{sol} = \int_{sep}^{SOL} -\langle\tilde{\mathrm{v}}_\mathrm{r}\tilde{\mathrm{p}}\rangle\frac{\partial\langle\mathrm{p}\rangle}{\partial \mathrm{r}}dr$ in the SOL. R_a characterizes the nature of the origin of SOL turbulence. When $R_a > 1$, the SOL width broadening is mainly induced by the turbulence spreading from the pedestal to the SOL. When $R_a < 1$, the SOL width broadening is due to locally produced SOL turbulence. If R_a~1, then effects of edge turbulence spreading, and local SOL production make comparable contributions. In this letter, we will focus on the impact of turbulence spreading from pedestal to the SOL on the heat flux width broadening.

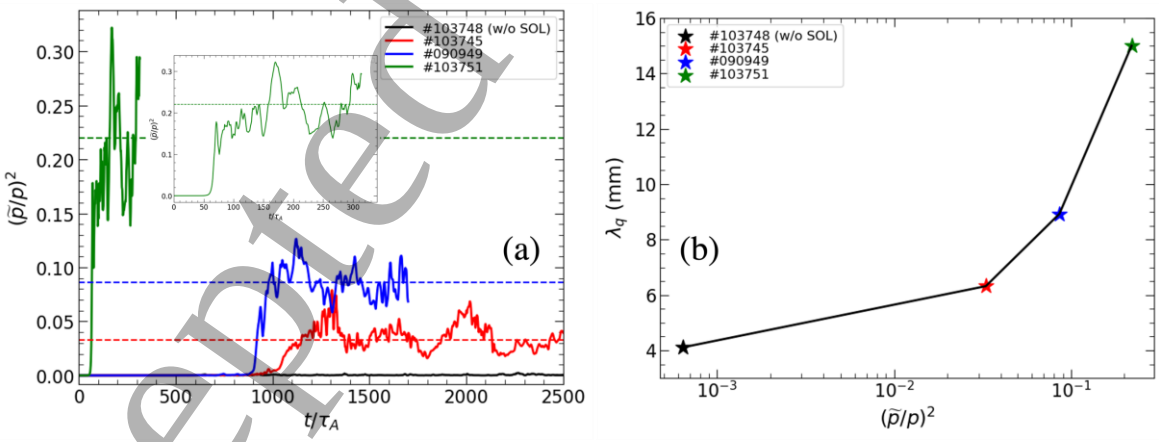

Fig. 2. (a) time evolution of fluctuation intensity at last close flux surface (LCFS); (b) heat flux width vs time averaged fluctuation intensity at LCFS in the nonlinear phase.

The BOUT++ six-field two-fluid turbulence code[34] is used to calculate the turbulence spreading and SOL width for EAST experimental equilibria with low poloidal magnetic field B_p = 0.16T for shot #090949 (small ELM) and high B_p = 0.21T for shot #103745 (small ELM), #103748(small ELM) and #103751 (large ELM). First, the flux surface averaged pressure

fluctuation intensity $(\tilde{p}/p)^2$ is calculated to investigate the relation between the edge turbulence and the SOL width λ_q. Fig. 2(a) shows the simulation results for the time evolution of pressure fluctuation intensity $(\tilde{p}/p)^2$ at the last closed flux surface (LCFS), 2(b) shows the divertor heat flux width calculated accordingly, for these 4 different EAST discharges. The ideal peeling-ballooning(P-B) mode is stable inside the pedestal for shot #103748 and there is no ELM crash, with flat SOL profiles.[35] The fluctuation intensity driven by drift modes is saturated at the lowest level in the nonlinear phase, as shown by the black curve. The diverter heat flux width is ~4 mm, as shown by the black star on the Fig. 2(b). The simulated λ_q is close to the value obtained from the Eich scaling law with $\lambda_q^{Eich}\sim 4.1mm$ [16] and calculated by the HD model with $\lambda_q^{HD}\sim 4.5mm$.[15] For shot #103745 and #090949, small ELMs are triggered by marginal P-B instability inside the pedestal.[19, 35] For shot 103751, the pedestal is unstable to the P-B mode, with large linear growth rate. A strong avalanche process occurs during the nonlinear phase, leading to a large ELM. The fluctuation intensity increases from the ELM-free to the small, and further to the large, ELM regime. The divertor heat flux width λ_q increases as the fluctuation intensity at the LCFS increases, as shown by Fig. 2(b). The resulting λ_q is larger than that calculated from the Eich scaling law. These simulation results show a trend consistent with experimental results (see Fig. 1). The BOUT++ simulated particle flux λ_{js} in the small/grassy ELM regime is comparable with EAST experimental measurements by probes[19]. It's worth noting that the simulated results for large ELMs correspond to the ELM crash phase, commonly referred to as the intra-large ELM phase. The measuring λ_{js} during the intra-large ELM phase in experiments can be challenging.

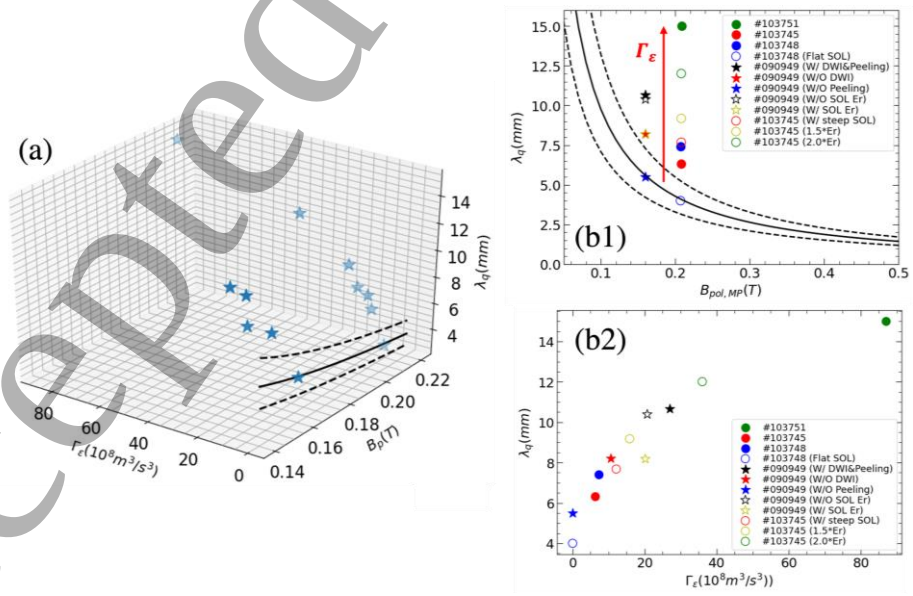

Fig. 3. (a) 3D plot of heat flux width $\lambda_q$vs poloidal magnetic field B_p and fluctuation energy density flux Γ_ε; (b) 2D plot of heat flux width λ_q vs poloidal magnetic field B_p (b1) and fluctuation

energy density flux Γ_ε (b2). The solid curves in (a) and (b1) are for the Eich scaling law[16] and the dashed curves are for the error bars.

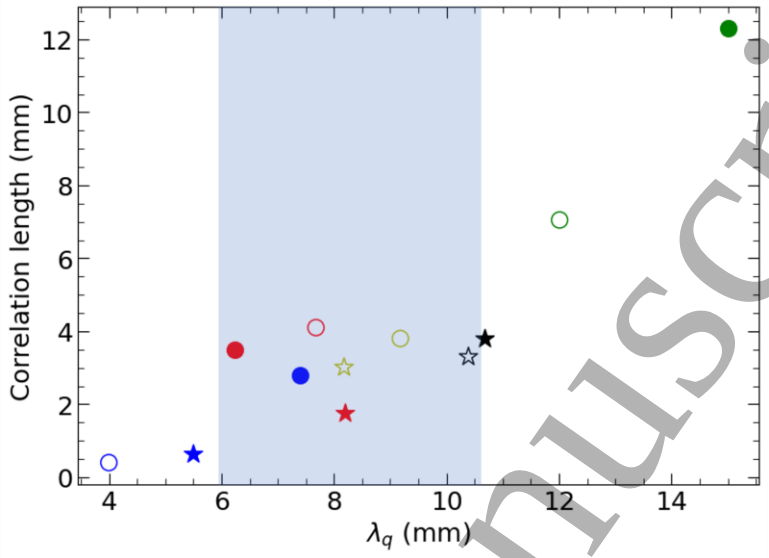

Fig 4. Radial correlation length of pressure fluctuation l_c vs. heat flux width λ_q.

To investigate how the turbulence generated in the pedestal spreads to the SOL, along with the correlation between the turbulence spreading and SOL width broadening, the fluctuation energy density flux $\Gamma_\varepsilon = c_s^2\langle\tilde{v}_r(\tilde{p}/p_0)^2\rangle$ is examined. The flux surface averaged and time averaged Γ_ε at LCFS in the nonlinear phase is calculated using the BOUT++ turbulence code. Fig. 3(a) shows 3D plot of the heat flux width λ_q vs poloidal magnetic field B_p and fluctuation energy density flux Γ_ε, while Fig. 3(b1) and (b2) are the corresponding 2D plots. If there is no ELM, the fluctuation level saturates at a low level, and the divertor heat flux width follows the Eich scaling law[16], as shown by the blue star and blue circle on the black solid curve of Fig. 3(b1). As the separatrix fluctuation energy density flux increases, the heat flux width is broadened significantly, for both high B_p (starts in Fig. 3(b1)) and low B_p (circles and bullets in Fig. 3(b1)). Fig. 3(b2) shows the relation between the heat flux width λ_q and fluctuation energy density flux Γ_ε scanned from the ELM-free to the ELM regimes. λ_q is significantly broadened by turbulence spreading from the ELM-free (blue circle for high B_p and blue star for low B_p) to the small-ELM (from red bullet to green circle in Fig 3(b2)) and further to the large ELM (green bullet) regime. P-B turbulence is especially effective at spreading, on account of its large effective mixing length as shown in Fig 4. In the ELM free regime, λ_q is small due to the small micro-turbulence mixing length l_c. In the small ELM regime, λ_q increases compared to ELM-free cases, likely due to the synergistic effects of the weak P-B and drift modes. The blue shaded region of Fig. 4, where significant scatter is observed, may be viewed as a cross-over regime between drift and turbulence

dominated regime. As the transition from the small to the large ELM regime takes place, λ_q exhibits an almost linearly increases as pressure fluctuation correlation length l_c increases.

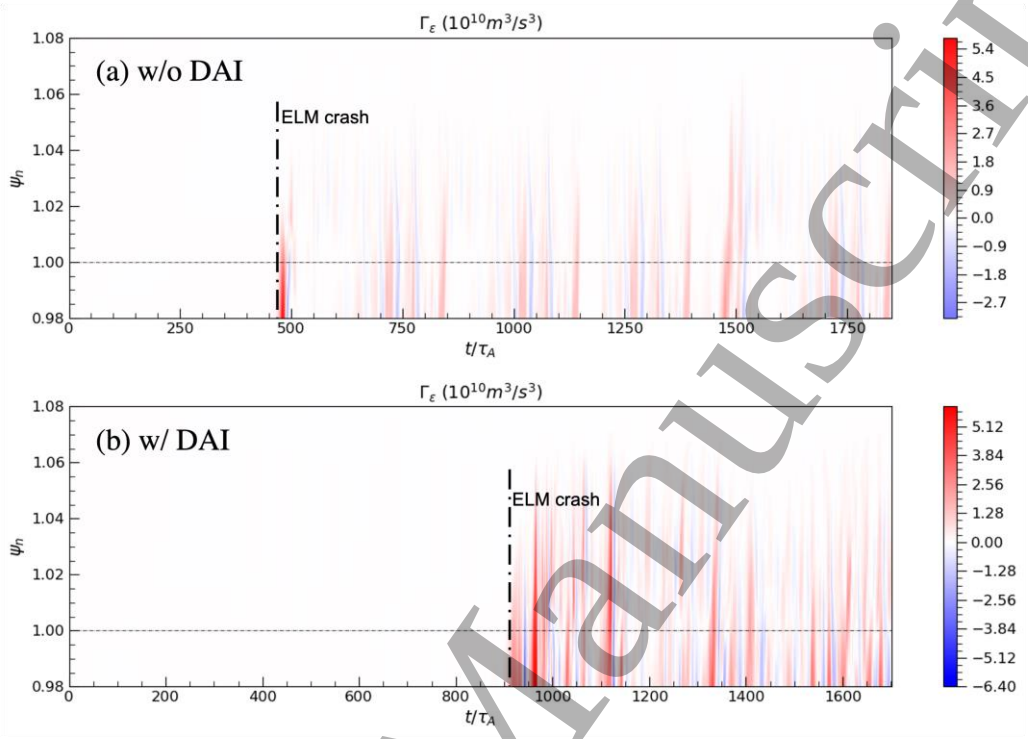

Fig. 5. Time evolution of fluctuation energy density flux for without (a) and with (b) drift-Alfvén instability.

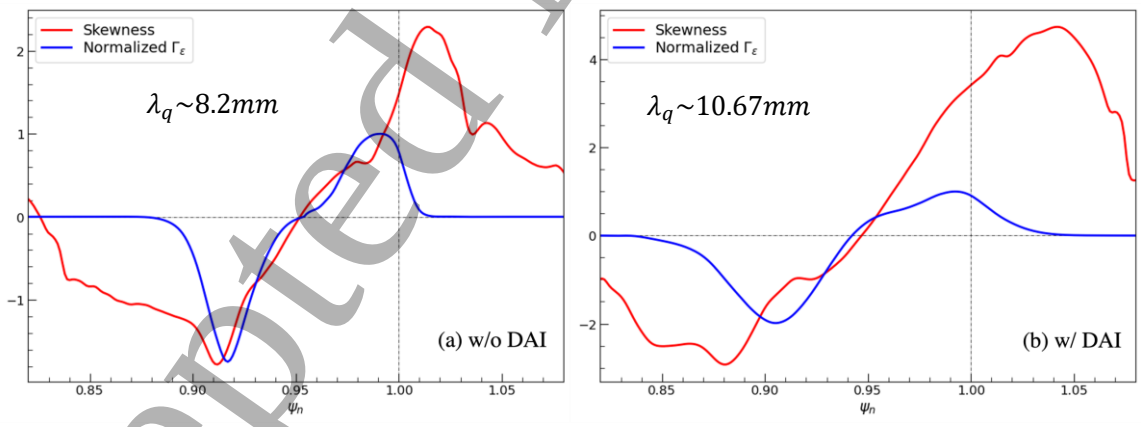

Fig. 6 Radial profiles of normalized fluctuation energy density flux Γ_ε (blue) and skewness (red) for without (a) and with (b) drift-Alfvén instability. Here fluctuation energy density flux is normalized to the max value for each case.

The fluctuation energy density flux Γ_ε is influenced by various factors such as the profiles of pedestal and/or SOL plasma, collisionality, and the radial electric field (Er) profile. Notably, the pedestal Er profile plays an import role in determining the pedestal instabilities. As depicted in Fig.3, for shot #103745, pedestal ExB flow shear increases from the red bullet to yellow circle and

green circle, resulting in increased turbulence spreading and ELM size. Conversely, when the SOL ExB shear near the separatrix increases, outward turbulence spreading is suppressed, and parallel transport is enhanced, leading to smaller λ_q in a small ELM regime, as demonstrated by the transition from the hollow black star to hollow yellow star in Fig.3. Furthermore, based on Eq. (4), and subsequent discussion, it is evident that both the spreading from pedestal to the SOL and local SOL turbulence production contribute to the broadening of the SOL width. BOUT++ simulations clearly demonstrate that the locally driven SOL turbulence, by steepening of SOL profiles, results in an increased broadening of the heat flux width. This effect is illustrated in Fig. 3, where the transition is observed from the blue circle to the blue bullet for shot #103748, and from the red bullet to the red circle for shot #103745. Overall, in the ELM-free regime, λ_q follows the Eich scaling law. However, in the ELM regime, λ_q is predominantly determined by the outward turbulence spreading at the separatrix. λ_q is broadened for increasing edge fluctuation energy density flux Γ_ε.[36] $\lambda_q \sim B_p^{-1}$ scaling persists for the broadened SOL.

Drift-Alfvén instability (DAI) and weak P-B instability play synergistic roles in the onset of ELM and turbulence spreading in the small ELM regime. There is no ELM triggered by DAI alone. λ_q follows the Eich scaling law, as shown by the blue star in Fig 3(b1) for shot #90949. The small ELM is triggered by P-B mode for cases both with (red star in Fig. 3b) and without DAI (black star in Fig. 3b). Without drift-Alfvén instability, the ELM crash driven by weak low-n peeling mode in the pedestal occurs rapidly (Fig.5(a)). The introduction of drift-Alfvén instability delays the onset of the ELM crash (Fig.5(b)) due to the mode-mode coupling.[37, 38] Following the ELM crash, the combination and interaction of large-scale P-B and small-scale drift-Alfvén modes enhance turbulence spreading. Fig.5 illustrates the intermittency resulting from a weak low-n peeling turbulence, characterized by the occurrence of sporadic events over time. The skewness of pressure fluctuations, S_p, shows strong correlation with the spreading flux,[39] suggesting the role of coherent fluctuation structures and the presence of intermittency in λ_q broadening, as depicted by Fig. 6. The spatial coincidence between the zero crossing of Γ_ε and the location denoted by $S_p \sim 0$ indicates the origin of turbulence, and its alignment with flux transport process. Positive S_p represents outward turbulence spreading with positive Γ_ε, while negative S_p represents inward turbulence spreading with negative Γ_ε. S_p near the separatrix is larger for the case with DAI, as compared to the case without DAI. Γ_ε increases as S_p increases. The time-averaged Γ_ε in the nonlinear saturated phase for with drift-Alfvén instability is $2.7 \times 10^9 m^3/s^3$, ~2.3 time larger than that without drift-Alfvén instability ($1.16 \times 10^9 m^3/s^3$). This leads to increased heat flux width broadening, as shown from the red star to black star in Fig. 3(b).

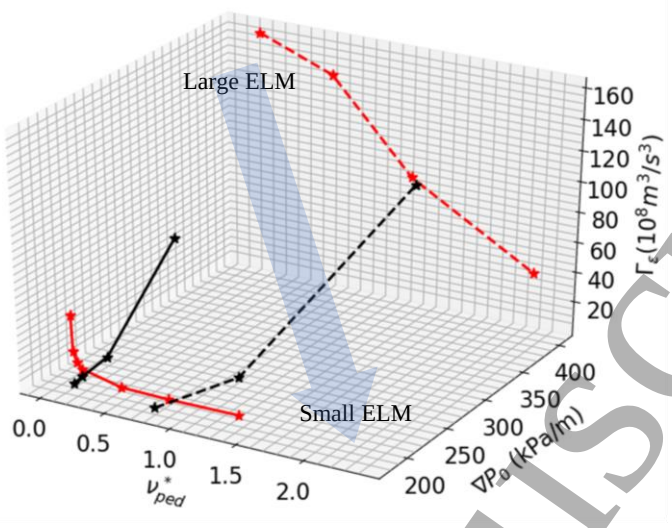

Fig. 7. 3D plot of fluctuation energy density flux Γ_ε vs pedestal peak pressure gradient ∇P_0 and υ^*_{ped};[35] black curves are ∇P_0 scan with low collisionality $\upsilon^*_{ped} = 0.108$ (solid curve) and high collisionality $\upsilon^*_{ped} = 1$ (dashed curve); red curves are υ^*_{ped} scan with small $\nabla P_0 \sim 200\ kPa/m$ (solid curve) and large $\nabla P_0 \sim 400\ kPa/m$ (dashed curve).

Having established that the heat flux width is broadened by enhanced turbulence spreading from the pedestal to the SOL, we now investigate how the pedestal parameters affect the fluctuation energy density flux Γ_ε. Scans of peak pedestal pressure gradient ∇P_0 and pedestal collisionality υ^*_{ped} are performed.[35] Fig. 7 shows the 3D plot of fluctuation energy density flux Γ_ε vs pressure peak gradient ∇P_0 and pedestal collisionality υ^*_{ped}. Here the black curves are ∇P_0 scans with low collisionality $\upsilon^*_{ped} = 0.108$ (solid curve) and high collisionality $\upsilon^*_{ped} = 1$ (dashed curve); while the red curves are υ^*_{ped} scans with small $\nabla P_0 \sim 200\ kPa/m$ (solid curve) and large $\nabla P_0 \sim 400\ kPa/m$ (dashed curve). The turbulence spreading from the pedestal to the SOL strongly depends on the pedestal plasma parameters ∇P_0 and υ^*_{ped}. The fluctuation energy density flux at LCFS increases as ∇P_0 increases and υ^*_{ped} decreases. This leads to the question of what is the physics mechanism for the drop of the fluctuation energy density flux Γ_ε as the pedestal collisionality υ^*_{ped} increases? BOUT++ nonlinear simulations indicate that turbulence spreading from pedestal to SOL depends on the radial mode structure from linear to nonlinear phase, since the latter sets the mixing length for transport. For high collisionality plasmas, the mode structure is narrower, so the effective mixing length and the outward turbulence spreading decrease, leading to lower fluctuation energy density flux Γ_ε. The low-n peeling mode induces more fluctuation energy flux Γ_ε for low collisionality, as compared to the high-n ballooning mode for high collisionality. This trend is due to the wider radial mode structure of the peeling mode. However, strong peeling turbulence can induce a larger type-I ELM crash and larger heat load on the divertor.

Thus, weak peeling turbulence – akin to MHD turbulence – such as occurs in the small ELM regime, is an attractive option.

In conclusion, improved confinement in H-mode leads to ExB shear suppression of SOL turbulence. As a consequence, the heat load width collapses to unacceptably narrow sizes and pessimistic scaling predicted by the HD model. We show that a state of weak MHD turbulence – as for small ELMs – is very attractive for SOL broadening driven by the transport of fluctuation energy from the pedestal to the SOL. The fundamental physics of the spreading process is elucidated in the letter. We demonstrate that λ_q is proportional to the fluctuation energy density flux Γ_ε at the last close flux surface (LCFS). Spreading is shown to be a multiscale process in the small ELM regime, which is enhanced by the synergy of large-scale P-B and small-scale drift modes. Pressure fluctuation skewness correlates well with the spreading flux, suggesting the role of coherent fluctuation structures and the presence of intermittency in λ_q broadening. The outward turbulence spreading from pedestal to the SOL is shown to be sensitive to pedestal parameters, such as pedestal pressure gradient ∇P_0 and pedestal collisionality υ^*_{ped}. The fluctuation energy density flux Γ_ε increases for increasing ∇P_0 and decreasing υ^*_{ped}. Peeling modes are seen to be especially effective for spreading on account of their large radial extent, which endows them with a large mixing length. The fluctuation energy density flux Γ_ε induced by low-n peeling modes, which dominate at low collisionality, is larger than for high-n ballooning modes, which occur at high collisionality, on account of the wider mode structure of the former. This research offers new insights into SOL width broadening driven by outward turbulence spreading in the small ELM regime and identifies key parameters and suggestions for experiments prior to ITER. To mitigate Type-I ELMs in the ITER baseline scenario, it is imperative to lower the pedestal pressure height, consequently entering a state of marginal plasma instability. This state is accompanied by the presence of weak MHD turbulence, ultimately leading to the broadening of the SOL width.[32] This strategic compromise emerges as the most optimal approach available to ITER for proficiently maintaining high-confinement conditions and effectively handling divertor heat exhaust.

This work was performed under the U.S. Department of Energy by Lawrence Livermore National Laboratory under Contract No. DE-AC52-07NA27344, LLNL-JRNL-845666 and by UCSD under Contract No. DE-FG02-04ER54738. This work was also supported by the Users with Excellence Program of Hefei Science Center, CAS under grant Nos. 2021HSC-UE014. The authors would like to express their gratitude for valuable discussions with X. Chu, Z. Y. Li, M. Y. Cao, T. Long, R. J. Hong, F. Khabanov, G. R. McKee, the BOUT++ team and the EAST pedestal experimental team.

References

[1] L.D. Landau and E.M. Lifshitz, 2013 Fluid Mechanics: Landau and Lifshitz: Course of Theoretical Physics, Volume 6. Elsevier.
[2] L. Prandtl, 1927 Turbulence Flow, NACA TM-435.
[3] T.S. Hahm and P.H. Diamond, 2018 J Korean Phys Soc 73, 747-792.
[4] T. Wu et al 2021 Plasma Sci. Technol. **23** (2), 025101.
[5] T. Estrada et al 2011 Nucl. Fusion **51** (3), 032001.
[6] P. Manz et al, 2015 Phys. Plasmas **22** (2), 022308.
[7] X. Garbet et al, 1994 Nucl. Fusion **34** (7), 963-974.
[8] O. D. Gurcan et al, 2006 Phys Rev Lett **97** (2), 024502.
[9] T. S. Hahm et al, 2004 Plasma Physics and Controlled Fusion **46**, A323-A333.
[10] V. Naulin et al, 2005 Phys Plasmas **12** (12), 122306.
[11] Z. Lin and T. S. Hahm, 2004 Phys. Plasmas **11** (3), 1099-1108.
[12] A. A. Townsend, 1949 Proceedings of the Royal Society of London Series A, Mathematical and Physical Sciences **197** (1048), 124-140.
[13] P. H. Diamond and T. S. Hahm, 1995 Phys. Plasmas **2** (10), 3640-3649.
[14] M. Sipos and N. Goldenfeld, 2011 Phys. Rev. E. **84** (3), 035304.
[15] R. J. Goldston, 2012 Nucl. Fusion **52,** 013009.
[16] T. Eich et al, 2011 Phys. Rev. Lett. **107** (21), 215001.
[17] G. S. Xu et al, 2019 Phys Rev Lett **122** (25), 255001.
[18] G. F. Harrer et al, 2022 Phys Rev Lett **129** (16), 165001.
[19] N.M. Li et al, 2022 Nucl. Fusion 62, 096030.
[20] G. Z. Deng et al, 2021Nucl. Fusion 61, 106015.
[21] X. Q. Xu, "Divertor Heat Flux Broadening by Grassy ELMs", in 28th IAEA Fusion energy conference (FEC 2020), https://conferences.iaea.org/event/214/contributions/17601/.
[22] A. Cathey et al, 2022 Plasma Physics and Controlled Fusion **64** (5), 054011.
[23] J. Garcia et al, 2022 Phys Plasmas **29** (3), 032505.
[24] M. Faitsch et al, 2021 Nuclear Materials and Energy 26, 100890.
[25] M. Faitsch et al, 2015 Plasma Physics and Controlled Fusion 57, 075005.
[26] H. J. Sun et al, 2022 Nuclear Fusion **63**, 016021.
[27] A. O. Brown and R. J. Goldston, 2021 Nuclear Materials and Energy **27**, 101002.
[28] N. M. Li et al, 2021 Nuclear Fusion **61** (2), 026005.
[29] T. Eich et al, 2020 Nuclear Fusion **60** (5), 056016.
[30] C. S. Chang et al, 2017 Nuclear Fusion **57**, 116023.
[31] Z. Y. Li et al, 2019 Nuclear Fusion **59** (4), 046015.
[32] X. Q. Xu et al, 2019 Nuclear Fusion **59** (12), 126039.
[33] N. M. Li et al, 2020 AIP Advances **10** (1), 015222.
[34] T. Y. Xia et al, 2013 Nuclear Fusion **53** (7), 073009.
[35] N. Li et al, 2022 Physics of Plasmas **29**, 122302.
[36] X. Chu et al, 2022 Nucl. Fusion 62 (6), 066021.
[37] P. W. Xi et al , 2014 Phys Rev Lett **112** (8), 085001.
[38] H. Seto et al, 2023 Comput. Phys. Commun. **283**, 108079.
[39] F. Khabanov et al, Statistical properties of turbulence at the edge of DIII-D L-mode positive and negative triangularity plasmas, the 32nd US Transport Task Force Workshop, May 32-35, 2023, Madison, Wisconsin, USA.